Mem. S.A.It. Vol. 76, 719

Memorie della

Solar variability: a brief review

M. P. Rast

High Altitude Observatory, NCAR, Boulder, CO 80307-3000, USA
e-mail: mprast@hao.ucar.edu

Abstract. This paper provides a brief review of solar particulate and radiative variability focusing on four topics: solar energetic particle events, cosmic ray modulation, total solar irradiance, and solar spectral irradiance. Magnetized plasma variability is discussed only in the context of energetic particle fluxes. Emphasis throughout is on the current understanding of the physical mechanisms responsible for the observed variability. References are representative, not comprehensive.

Key words. Sun: variability – Sun: total solar irradiance – Sun: solar spectral irradiance – Heliosphere: cosmic ray modulation – Heliosphere: solar energetic particles

1. Introduction

The Sun's particulate and radiative outputs display variability on a wide range of spatial and temporal scales. The observed radiative variability is largely, perhaps completely, due to the temporal evolution of the magnetic fields threading the solar surface and the motion of these nonuniform fields with respect to a fixed observer as a consequence of the solar rotation. The observed particulate variability results indirectly from changes in the heliospheric magnetic field, which modulates the galactic cosmic ray flux, and directly from changes in the solar plasma outflow depending on the level of solar magnetic activity. In this paper we briefly discuss four topics in solar particulate and radiative variability: solar energetic particle events, cosmic ray modulation, total solar irradiance variation, and solar spectral irradiance variation. Magnetized plasma variability (that for example due to coronal mass ejections and solar wind interactions) is discussed only in the context of energetic particle fluxes. We focus on current understanding of the physical mechanisms governing the observed behaviors. The discussion is necessarily brief, incomplete, and without full historical development. Consequently, references are mainly to recent reviews, within which the reader may find more complete discussions and more comprehensive citations.

2. Solar particulate variability

Energetic particles observed at the Earth have two main sources: distant supernovae and the nearby Sun. Galactic cosmic rays are accelerated in supernovae shocks and have energies to > 30GeV. Solar energetic particles are accelerated to energies of $\sim$10KeV to $\sim$300MeV during magnetic reconnection in solar flares or in shocks produced by the interaction between coronal mass ejections and the solar wind. The flux of both galactic cosmic rays and solar energetic particles are modulated by the solar magnetic activity cycle.

2.1. Solar energetic particle events

Solar energetic particles can plunge deep into Earth's polar mesosphere and upper stratosphere, causing increases in NO_x concentrations and consequent catalytic destruction of O_3. Energetic particle events, during which particle fluxes can rise by many orders of magnitude for periods of days, can have effects on stratospheric ozone concentrations lasting months to years (Rusch et al. 1981, Reid et al. 1991, Jackman et al. 1999, 2001). These events appear to be of two types (sometimes mixed) associated with distinct sources and acceleration processes (Reames 1999, Figure 1). Impulsive events are believed to originate with particle acceleration by resonant wave-particle interactions at solar flare sites. The presence of high ionization states and the enhancement of the $^3He/^4He$ and Fe/O ratios over coronal values suggest that the particles originate from a small region of hot ($> 10^7$K) plasma magnetically connected to the observer. Gradual events, on the other hand, originate with fast coronal mass ejections which form shocks in the solar wind. These events display elemental abundances and ionization states characteristic of the ambient $1 - 2 \times 10^6$K solar corona and wind, with high particle intensities occurring over a wide range of solar longitudes for several days. Most large solar energetic particle events are of this second type.

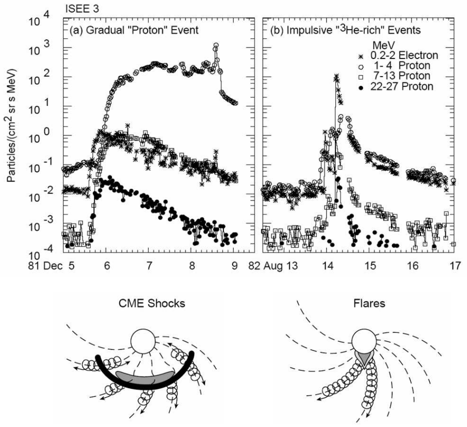

Fig. 1. Solar energetic particle events are of two types. In (*a*), energetic particle fluxes during a coronal mass ejection without significant flaring. In (*b*), particle fluxes during a flare unaccompanied by a coronal mass ejection. Sketches below the time traces illustrate the extent of the source regions for the two acceleration processes. All images from Reames (1999).

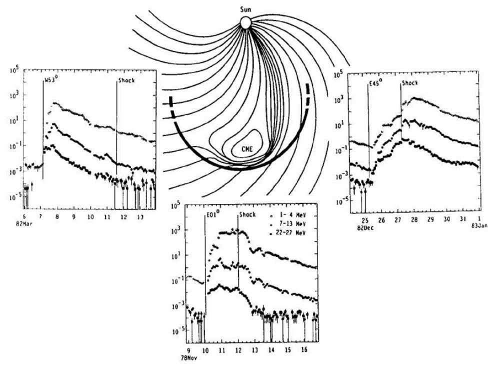

Fig. 2. The temporal evolution of the solar energetic particle intensity depends on the positioning of the observer with respect to coronal mass ejection shock and the magnetic connectivity between the two. From Reames (1999).

Shock accelerated energetic particle spectra depend, not only on the interaction between the coronal mass ejection and the solar wind and thus the temporal evolution and spatial structure of the shock itself, but also on the magnetic connectivity of the shock region with the observer (Reames 1999, Figure 2). The most significant particle acceleration occurs in the strong shock region just ahead of the coronal mass ejection where the flow speeds are highest. Due to the spiral structure of the heliospheric magnetic field (§2.2), observers on the eastern flank of the shock (left in Figure 2) are magnetically connected to the strong shock region well before shock passage. The opposite is true of observers on the western flank. Thus peak energetic particle intensity can occur before, after, or nearly simultaneous with shock passage depending on the solar longitude at which the coronal mass ejection is observed. The intensity-time profile of any individual solar energetic particle event largely traces the temporal evolution of the observers magnetic connectivity with the shock region.

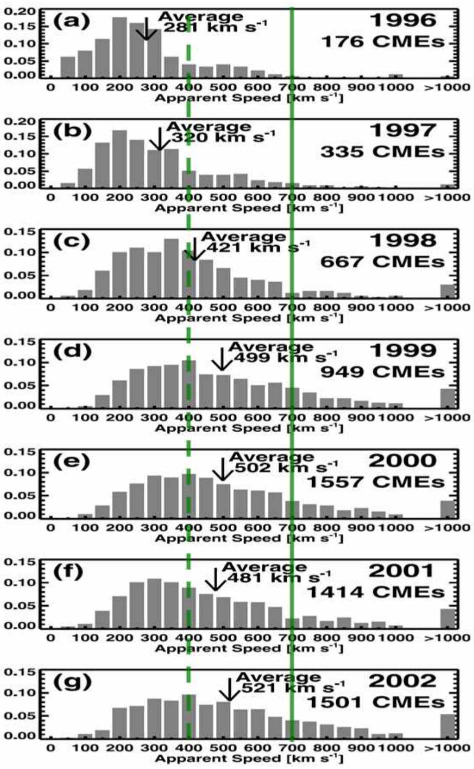

Fig. 3. The number and speed of coronal mass ejections (CMEs) depends on the phase of solar cycle (progressing in this figure, top to bottom, from solar minimum to solar maximum). Only a fraction of all coronal mass ejections have sufficient speed to shock the solar wind. *Dashed* and *solid* lines indicate typical slow and fast solar wind speeds. Figure from Yashiro et al. (2004).

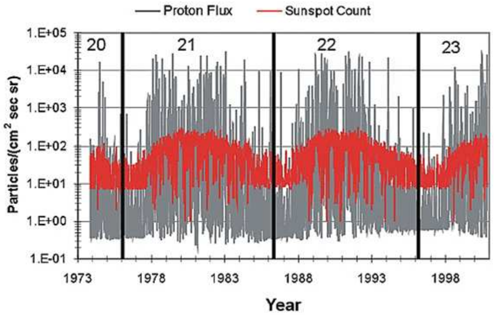

Fig. 4. Sunspot number (*dark*) and integrated (0.394 – 440MeV) proton flux (*grey*) as a function of time, as measured by the Charged Particle Measurement Experiment onboard the Interplanetary Monitoring Platform 8. Figure from Simunac & Armstrong (2004).

Since the slow and fast solar wind components have speeds of ~ 400km/s and $\sim 600 - 800$km/s respectively, only the fastest coronal mass ejections have speeds sufficient to shock in the solar wind and cause solar energetic particle events. Since both the number and the speed of coronal mass ejections increase with increasing solar activity (Yashiro *et al.* 2004, Figure 3), so to do the number of solar energetic particle events observed. Interestingly however, their number peaks not at solar maximum, as might be expected, but during the rising and declining phases of the solar cycle (Simunac & Armstrong 2004, Figure 4). This double peak is also seen in ice-core nitrate concentrations (Ogurtsov et al. 2004), which additionally reflect strong individual particle events (some associated with known historic white light flares) and long term trends well back in time (McCracken et al. 2001a,b). The cause of the double peak may be related to the latitudinal distribution of coronal mass ejections on the Sun. They are confined to the equatorial streamer belt during solar minimum but extend to high latitudes in the multipole configuration of solar maximum (Yashiro et al. 2004). This could lead to a reduction in the number of geoeffective particle events during solar maximum despite an absolute increase in the number and speed of coronal mass ejections. Preliminary estimates from the published latitudinal distribution histograms (Yashiro et al. 2004) however suggest that this is not the case. Another possibility is that both the measured charged particle flux and the ice-core nitrate concentration are sensitive to low energy galactic cosmic rays. As will be discussed below, galactic cosmic rays are modulated by the heliospheric magnetic field is a way that reduces their flux during solar maximum (Figure 5). If some of the presumed solar energetic particle signal is actually due to galactic cosmic rays, the reduced galactic cosmic ray flux at solar maximum, combined with an actual increase in solar energetic particle events, may explain the observed double peak.

2.2. Cosmic ray modulation

High energy galactic cosmic rays (above the geomagnetic shielding limit; above 1 – 15GeV pole to equator) can penetrate deep into Earth's atmosphere altering isotopic concentrations in the stratosphere and troposphere and leaving behind a trail of ionized particles. The cosmogenic isotopes are incorporated into ice, ocean, and biomass deposits leaving a record of the galactic cosmic ray flux, while the ionized particles may directly or indirectly modify cloud nucleation processes providing a link between solar activity and terrestrial weather and climate (Dickinson 1975). The possibility of such a link has lately received considerable attention (eg. Svensmark & Friis-Christensen 1997, Tinsley 2000, Marsch & Svensmark 2000*a*, *b*, Sun & Bradley 2002, Kazil & Lovejoy 2004), and debate continues about both its operation and importance. Notwithstanding, isotopic measures of cosmic ray modulation provide the most direct measure of solar variability into the pre-scientific past.

Galactic cosmic rays are thought to be accelerated primarily in supernovae shocks. Their apparently isotropic flux into the heliosphere suggests that the interstellar medium is filled with highly structured magnetic fields which scramble the source direction by imposing a convoluted path on the charged particles as they travel from the shock acceleration site to the heliopause. Since massive rapidly aging stars are the primary source of supernovae explosions, the galactic cosmic ray flux into the heliosphere is expected to be modulated by a factor of $\sim 0.25-1.35$ on a time scale reflecting the interval between galactic spiral arm crossings ($\sim 140\times10^6$yr) during which compression of the interstellar medium triggers increased star formation in the local solar neighborhood (Shaviv 2002). A true constancy of the galactic cosmic ray flux into the heliosphere, or a detailed understanding of the causes of any inconsistency, is of course needed if one is to employ cosmic ray modulation (and surrogate isotopic concentrations) to infer solar variability.

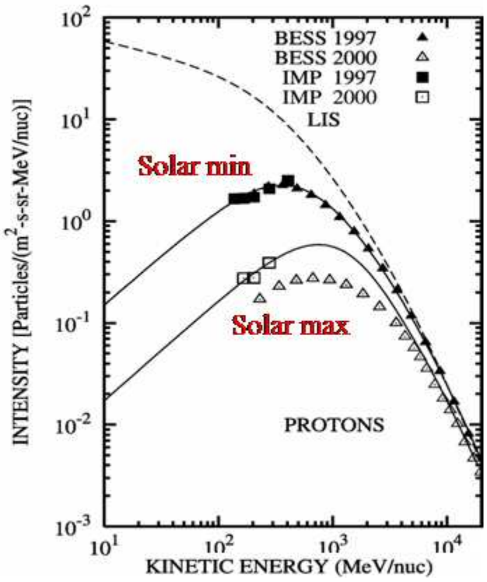

Fig. 5. Galactic cosmic ray intensity spectra observed at Earth around the time of solar minimum (*filled* symbols) and solar maximum (*open* symbols). *Dashed* curve is an assumed interstellar spectrum. Figure from Caballero-Lopez et al. (2004).

Once produced, galactic cosmic rays must make their way into the inner heliosphere along heliospheric magnetic field lines. Collisions of cosmic rays with the ambient plasma are negligible, so the heliospheric field determines their motion. Similarly, the magnetic field itself is frozen into the highly conductive solar wind plasma and so it is carried outward by the wind. Under these conditions four main processes contribute to cosmic ray transport: diffusion of the cosmic rays inward along magnetic field lines at a rate limited by scattering of the charged particles from small scale magnetic irregularities, advection of the magnetic field, and therefore the cosmic rays, outward by the solar wind, gradient and curvature drifts imparting global scale motions depending on the large-scale heliospheric field configuration, and adiabatic work by radial expansion or shock compression resulting in energy transfer between the cosmic ray particles and solar wind plasma. These processes are summarized by Parker's transport

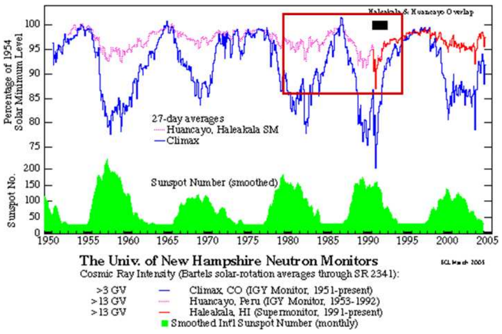

Fig. 6. Cosmic ray intensity is anti-correlated with solar activity. Alternate cycles show more or less sharply peaked intensity maxima. The *box* delineates the time series used by Marsch and Svensmark (2000*a*) to support a strong correlation between galactic cosmic ray flux and low cloud cover. It would be interesting to know whether this correlation persists over adjacent cycles. Figure from http://ulysses.sr.unh.edu .

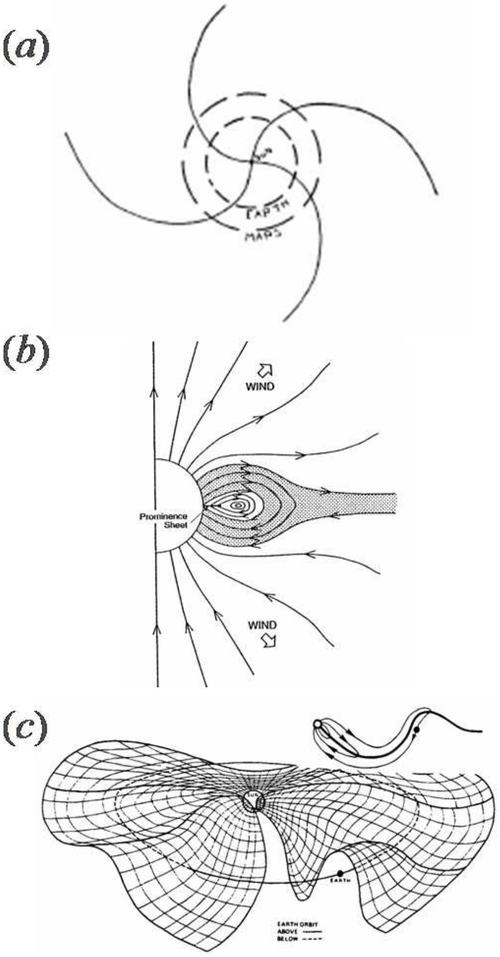

Fig. 7. (*a*) Solar rotation combined with solar wind advection draws the heliospheric magnetic field out into Archimedean spiral (equatorial plane shown). Figure from Parker (1958). (*b*) Open field lines meet in an equatorial current sheet (axial plane shown). Figure from Low (1996). (*c*) The equatorial current sheet becomes increasingly wavy before magnetic field reversal at solar maximum. Figure from Kelley (1989).

equation governing the quasi-isotropic distribution function (locally isotropic velocity distribution), $f(\mathbf{x}, p, t)$, for cosmic rays of momentum p at position $\mathbf{x}$ and time t (Parker 1965, Jokipii 1991):

$$\frac{\partial f}{\partial t} = \frac{\partial}{\partial x_i}\left(\kappa_{ij}\frac{\partial f}{\partial x_j}\right) - U_i\frac{\partial f}{\partial x_i} - V_{di}\frac{\partial f}{\partial x_i} + \frac{1}{3}\frac{\partial U_i}{\partial x_i}\left(\frac{\partial f}{\partial \ln p}\right) + S\,(x_i, p, t)\,, \qquad (1)$$

where S represents the outer heliospheric boundary source.

The time scales for cosmic ray equilibration in and solar wind transit of the heliosphere are on the order of $1 - 3$ years. For this reason a first approximation to cosmic ray modulation solves Equation 1 in the static limit and looks at solutions for differing magnetic field configurations depending on the phase of the solar cycle. If cosmic ray diffusion inward is balanced by solar wind advection outward, an analytic spherically symmetric solution, the force – field solution, can be obtained (Gleeson & Axford 1968). In this case the observed reduction in cosmic ray intensity at solar maximum (Figure 5) is either due to an increase in the average solar wind speed or a decrease in the diffusion coefficient (increased small scale scattering). While these processes may be important and are likely variable over solar cycle, such a simplified model does not explicitly take into account the heliospheric field configuration and can not therefore explain observations that depend on it. One of the most intriguing of these is that alternate solar cycles display

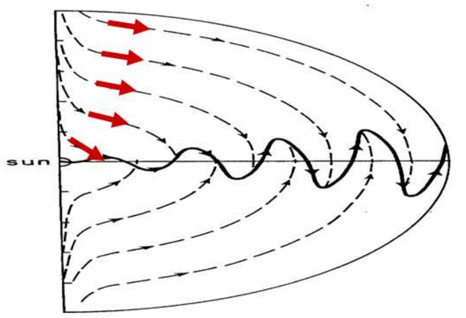

Fig. 8. Combined curvature and gradient drift directions for a positively charged cosmic ray particle in a heliospheric field configuration idealizing that of solar minimum with the dipolar field oriented so that the north polar fields point outward from the Sun. Particles drift in from the heliospheric poles and are ejected rapidly outward along the equatorial current sheet. Alternate solar cycles induce oppositely signed drift motions. Figure from Jokipii (1991).

characteristically different cosmic ray intensity profiles (Figure 6), reflecting cycle dependent large-scale cosmic ray drift motions.

The heliospheric magnetic field configuration is determined by the inner magnetic boundary condition at the Sun and the solar wind. Solar rotation combined with radial advection of the magnetic field by the solar wind configure the heliospheric field in an Archimedean spiral (Parker 1958, Figure 7*a*), with the field pointing inward in one hemisphere and outward in the other, defining a current sheet in the equatorial plane (Figure 7*b*). The current sheet is not completely flat nor azimuthally symmetric due to continually evolving irregularities in the distribution of surface magnetic fields, and the waviness (Figure 7*c*) of the current sheet increases towards solar maximum as it rotates to accommodate the change in sign of the global field.

The global heliospheric field configuration leads to large scale cosmic ray drifts of magnitude comparable to or greater than the motions due to solar wind advection and inward diffusion (Jokipii 1991). The drift motions carry cosmic ray particles inward or outward along the equatorial current sheet depending on the direction of the field and sign of the charged particles (Jokipii 1991, Figure 8). Since the global solar field reverses every 11 years, the heliospheric boundary origin of the galactic cosmic rays and the drift directions also do so. This is the only physical mechanism that can produce the distinctive alternate-cycle effects in the observed cosmic ray modulation (Lockwood & Webber 2005).

3. Solar radiative variability

The presence of magnetic fields in the solar photosphere, chromosphere, and corona affects the thermodynamic structure and stratification of the solar atmosphere. As a consequence of the horizontal inhomogeneities in the field, an image of the Sun at any given wavelength is a composite of the solar atmosphere at differing heights depending on the emissivity or absorptivity of the horizontally inhomogeneous plasma at the wavelength of observation. This results in distinctly different appearances of the Sun at differing wavelengths (Figure 9), and in combination with with magnetic field evolution and solar rotation, yields wavelength dependent variability.

3.1. Total solar irradiance

Total solar irradiance is a measure of the spectrally integrated incident solar energy per unit area at one astronomical unit. It is dominated by the solar visible, near ultraviolet, and near infrared radiation. For more than 25 years precise measurements of the total solar irradiance have been made from space. These observations can be combined to produce a single composite time series (Fröhlich & Lean 2004, Figure 10), but since multiple spacecraft data sets are involved, such composites are sensitive to modeled instrumental degradation and data matching techniques. As a result, small but important differences (eg. secular trends) exist between results obtained by different groups. All of them, however, show peak to peak total solar irradiance changes of ~0.06 − 0.07 % over the last three solar cycles. This variation can be largely accounted for by a combination of strong downward excursions (reduced total solar irradiance) due to disk passage of sunspots

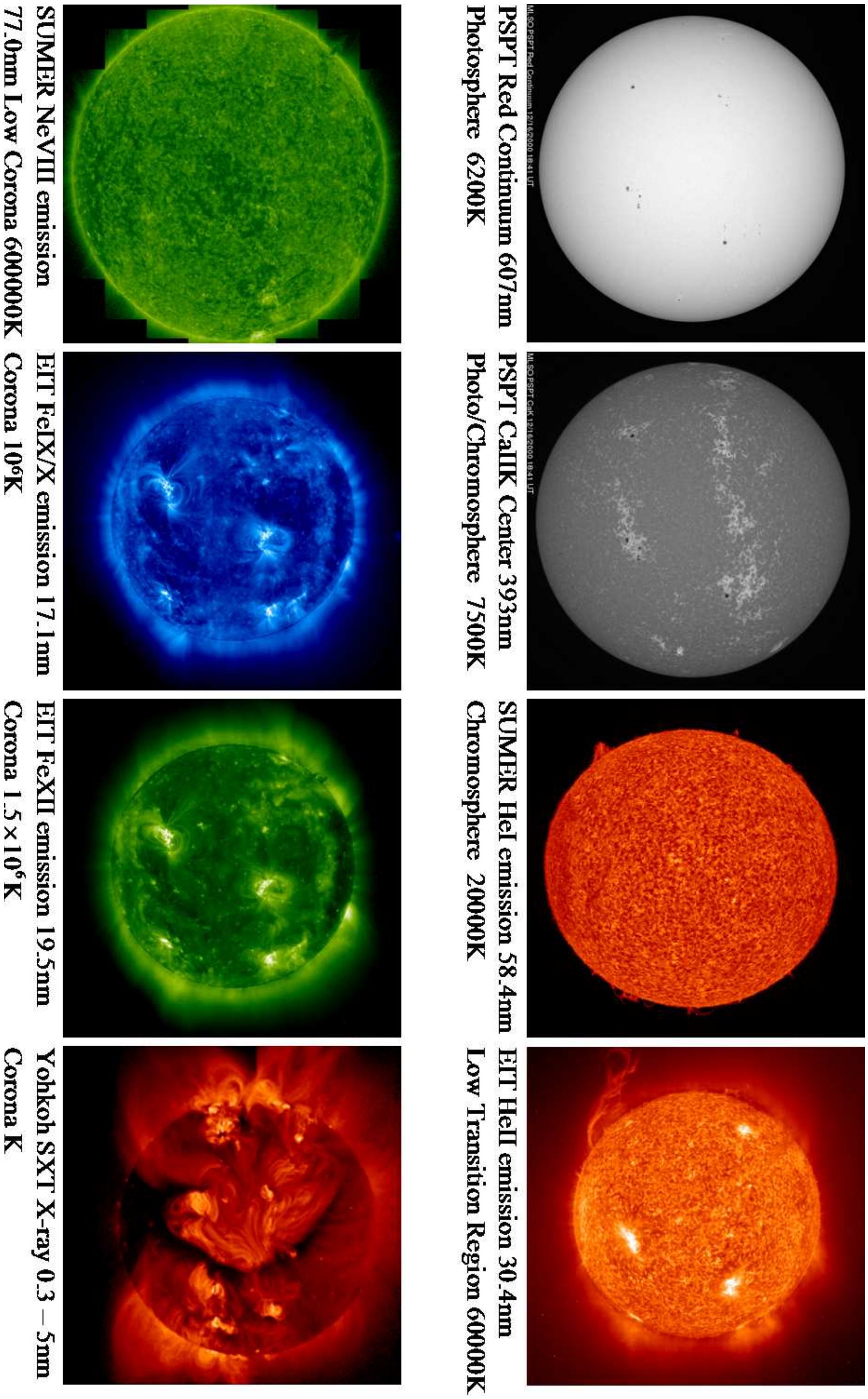

Fig. 9. The appearance of solar magnetic features depends critically on the wavelength at which they are observed. Solar variability, due to the evolution of the magnetic fields with time and the rotation of the Sun with respect to the observer, is thus wavelength dependent.

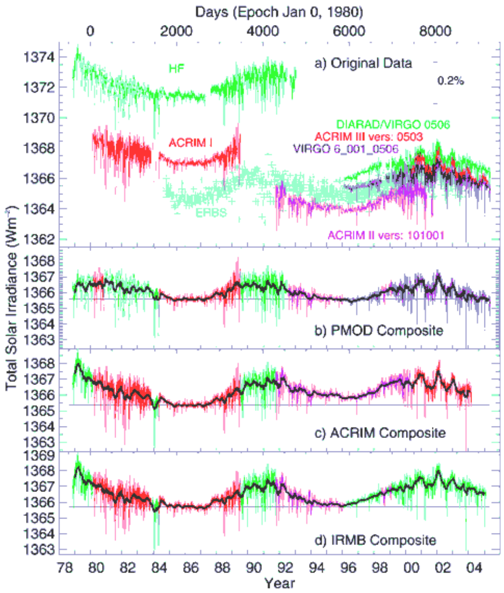

Fig. 10. Composite daily averaged total solar irradiance time series (*grey* curve in lower three panels) and their 81 day running averages (*black* curves in lower three panels) as derived from space craft radiometer data (top panel) by separate research groups (see Fröhlich & Lean (2004) for details). Small but significant differences between the composite time series are apparent. Figure from http://http://www.pmodwrc.ch .

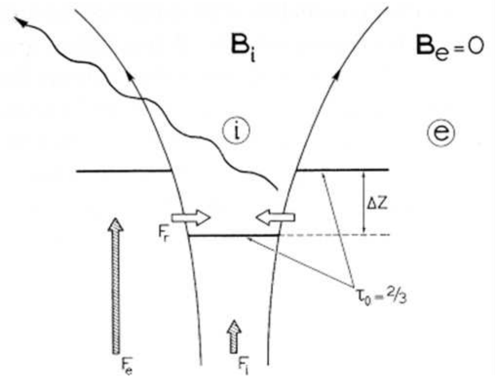

Fig. 11. Schematic of a magnetic flux tube in the solar photosphere, showing the depressed optical depth surface ($\tau = 2/3$), the suppressed convective flux ($F_i < F_e$), and the lateral heating (F_r) within the structure. Figure from Schrijver & Zwaan (2000).

and significant upward excursions (increased total solar irradiance) due to the presence of bright facular/plage regions on the solar disk. During solar activity maximum the average increase in facular brightening more than compensates for sunspot darkening, resulting in a net increase in total solar irradiance.

Why do sunspots appear dark and faculae bright at the near infrared, visible, and near infrared wavelengths that dominate total solar irradiance measurements? Two competing effects contribute to the observed intensity of solar magnetic structures: reduced radiative opacity and suppressed convective transport. Since the magnetic field exerts a supporting force on the ionizing plasma within a magnetic flux concentration, the gas pressure and therefore the continuum radiative opacity there is reduced. Consequently one sees slightly deeper into the solar photosphere in regions where the magnetic flux density is higher, causing the magnetic structure to appear brighter than its surroundings. Moreover, radiation enters the low opacity interior of the flux concentration laterally from the walls. When the width of the object exceeds the photon mean free path (∼ 100km) an internal radial temperature/intensity gradient developes, causing the structure to look brighter when viewed from an angle than when viewed directly (Spruit 1976, Figure 11, the 'hot-wall' model). Thus faculae appear brighter than their surroundings and display a center-to-limb intensity variation the details of which which depend on the observation direction and their interior structure.

Since the photon mean free path also governs the depth of the photospheric boundary layer, and therefore the convective downflow plume width, at about the same size at which lateral radiative heating of the interior of a magnetic flux concentration becomes inefficient the object also begins to interfere with vertical transport of heat by convection. While small magnetic flux concentrations are advected by the turbulent flows in the photosphere, ultimately ending up in the convergent boundaries and vertices between supergranules (the solar magnetic network), large magnetic structures inhibit the convective motions locally, reducing the transport of heat from

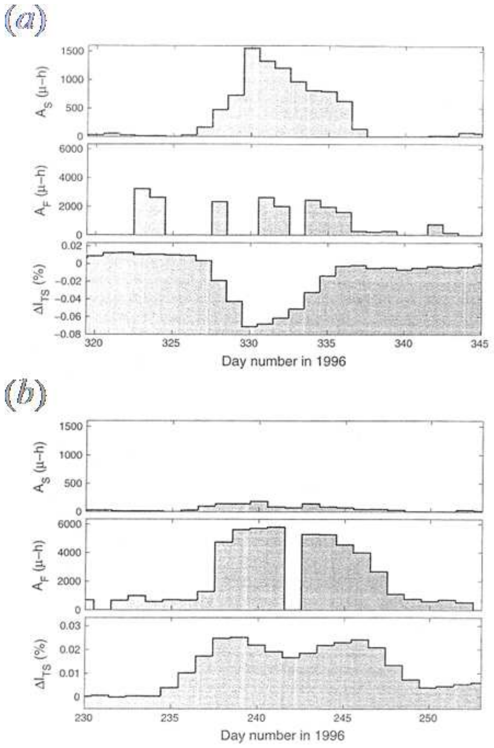

Fig. 12. Passage of a spot dominated (*a*) and a faculae dominated (*b*) active region across the solar disk, showing the sunspot area (*top*), facular area (*middle*), and total solar irradiance perturbation (*bottom*) for each. Figure from Lockwood (2005).

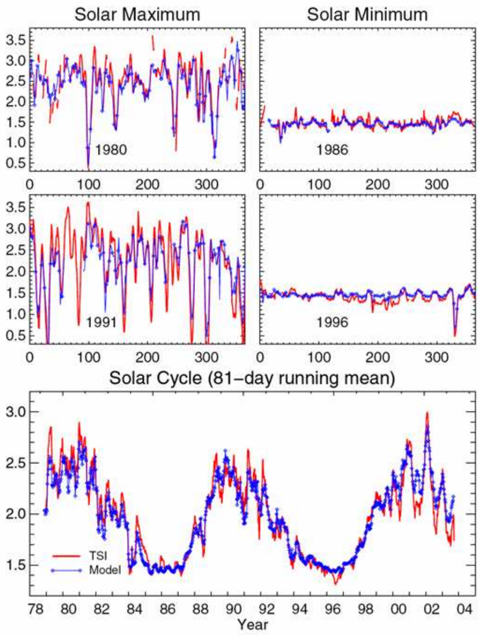

Fig. 13. Empirical reconstruction (*dark* curves) of the total solar irradiance variability (*light* curves) for low and high solar activity periods using sunspot observations and a facular proxy. Bottom panel shows smoothed measurements and model results for a period spanning two solar cycles. Figure from Fröhlich & Lean (2004).

the solar interior with a consequent decrease in their internal temperature. Thus pores and sunspots appear darker than their surroundings.

Figure 12 plots the change in total solar irradiance during disk passage of two active regions, one (Figure 12*a*) dominated by a sunspot and the other (Figure 12*b*) by faculae. Also shown for each are the disk areas occupied by the sunspot or faculae. The decrease in total solar irradiance due to sunspot disk passage occurs in phase with its area. The larger the projected area of the spot on the disk the deeper the irradiance perturbation. The total solar irradiance increase due to facular brightening (Figure 12*b*) is not as tightly correlated with facular area. Because of their center-to-limb variation, faculae near disk center and very close to the limb have extremely low contrast with the surrounding quiet Sun and are therefore very difficult to identify in the visible continuum. As a consequence the measured facular area falls to zero as the active region crosses disk center and also quickly toward zero when it is close to either limb. Despite this apparent decrease in disk coverage, the facular contribution to the measured total solar irradiance perturbation remains significant (*lower* panel Figure 12*b*).

This inability to identify the presence of low contrast features on the Sun, despite their significant contribution to total solar irradiance, is critical for models that attempt to deduce irradiance variations by summing over magnetic structure contributions. The problem can be largely avoided by identifying the magnetic structures, either with proxy indices or in images, in wavelengths at which their contrast is large. This generally means observing in a wavelength at which chromospheric emission is high to deduce the facular contribution, and empirical models using sunspot observations and a chromospheric facular proxy (eg. the MgII index) can account for 77% (or more) of the observed total solar irradiance variance simply by regressing the sunspot and facular areas (or indices) against the observed irradiance (Fröhlich & Lean 2004, Figure 13). This remarkable fact suggests that perhaps all solar radiative variability results from photospheric modulation of radiative losses by the presence of surface magnetic structures with no accompanying deep rooted structural changes within the Sun. The upcoming Centre National d'Etudes Spatiales micro-satellite mission Picard, to be launched in 2008, will attempt to address this issue directly with a combination of irradiance, helioseismic, and solar diameter measurements (Thuillier et al. 2003).

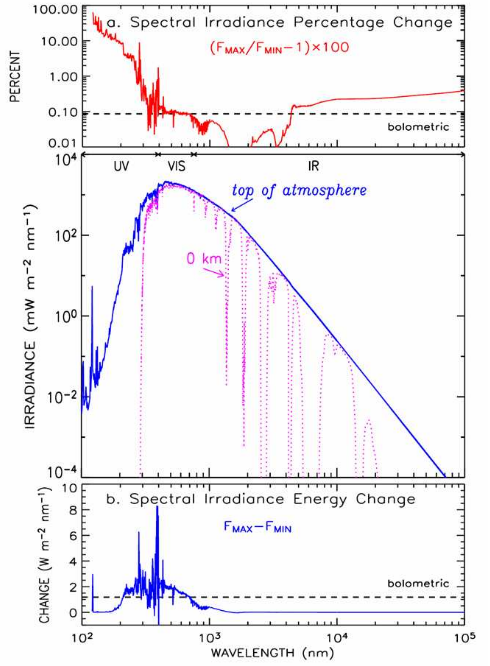

Fig. 14. Solar spectral irradiance (*middle* panel) at the top of the Earth's atmosphere (*dark* curve) and at the Earth's surface (*light* curve). Absolute (*bottom* panel) and relative (*top* panel) irradiance change over a solar activity cycle as a function of wavelength. Figures from Fröhlich & Lean (2004).

3.2. Solar spectral irradiance

Although the total solar irradiance is dominated by near infrared, visible, and near ultraviolet radiation from the Sun, the amplitude of the variability is greater at shorter wavelengths (Figure 14). This increase at short wavelengths is due to the temperature and density structure of the solar atmosphere. Figure 15*a* plots the temperature and density of a model solar atmosphere as a function of height, along with the formation height of lines often used for solar observations. Visible radiation largely originates in the solar photosphere, with ultraviolet and x-ray radiation having their sources in the chromosphere, transition region, and corona. Within magnetic structures, both the increased temperature and decreased density require a steeper temperature increase with height so that the downward conduction of heat can balance radiative loss. The larger the magnetic flux density the smaller the atmospheric temperature scale height, resulting in an increase in the temperature/intensity contrast between the structures with increasing height (Figure 15*b*). Even sunspots become bright compared to their surroundings in the upper chromosphere, since convective suppression no longer plays a role in determining their temperature structure. As the magnetic fields evolve or the Sun rotates, the increased contrast of the magnetic features with height yields increased radiative variability in wavelengths at which the radiation has a chromospheric or coronal origin.

Two component empirical models based on sunspot and facular indices, derived either from chromospheric proxies or images, reproduce solar ultraviolet variability better at shorter wavelengths than longer ones (Fröhlich & Lean 2004). They do so, however with less of the total variance explained than when total solar irradiance variations are similarly modeled. This is because the details of the spectral irradiance variability amplitude and phasing depend critically on the observed structures, their position, and the wavelengths at

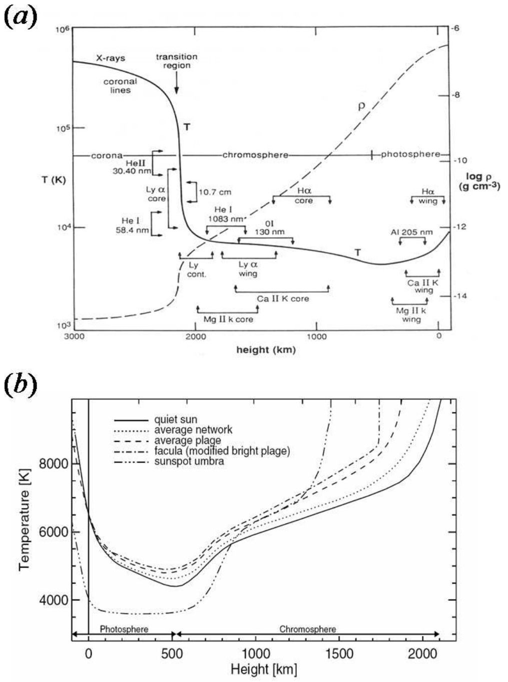

Fig. 15. In (*a*), temperature and density profiles in a model solar atmosphere and the approximate formation heights of selected lines and continua. Figure from Avrett (1992). In (*b*), magnetize atmosphere models of Fontenla et al. (1999) indicating the increased temperature contrast between magnetic structures with height. Figure from Fröhlich & Lean (2004).

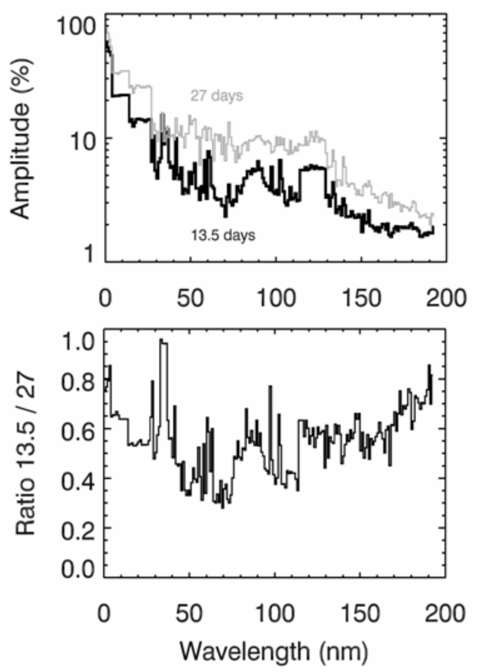

Fig. 16. Solar variability at full and half rotational periods as a function of observation wavelength. Half-period (13.5 day) variability is enhance at wavelengths that are strongly limb brightened (coronal emissions off limb) *and* at those that are strongly limb darkened (ultraviolet emission at disk center). Figure from Woods et al. (2005).

which they are observed. These are not easily captured by simple proxy models. As an example, consider the observed full and half solar rotation period variability observed by the Solar EUV Experiment as a function of wavelength (Woods et al. 2005, Figure 16). Short wavelength coronal emissions have an elevated 13.5day periodicity because prominent structures off the limb rotate limb to limb in one-half rotation period. By contrast, the elevated 13.5 day periodicity in the far ultraviolet is greatest at those wavelengths with the largest center to limb darkening. Here the half-period power is due to the appearance and disappearance of active regions as they cross the disk. In order to empirically reproduce the solar spectral variability the atmospheric structure of all components must be known well enough to synthesize their spectral contributions, as a function of viewing angle, over broad and well resolved wavelength bands.

The focus of solar radiative variability research depends sensitively on one's primary interest. Interest in the coupling between solar output and terrestrial climate motivates the question of what amplitude variation occurs on what time scales at what frequencies. This question is best addressed by observations aimed at the spectral mapping of solar magnetic structures over broad but well resolved wavelength bands to understand the Sun's spectral output as a function of the magnetic flux density and structure size distribution on its surface. The frequencies observed should be informed by climate sensitivity. Interest in the underlying physical origin of solar radiative variability itself motivates the question of whether all the observed variability is due to surface modulation of radiative loss by magnetic structures or also reflects some additional as yet unknown thermal modification of the interior. This question is best address by observations that aim at disentangling surface effects from deeper rooted causes by simultaneously measuring the surface magnetic fields and photometric intensity in high spatial resolution images. For this purpose infrared observations which penetrate the deep photosphere at the opacity minimum should accompany those made in the visible.

Acknowledgements. The National Center for Atmospheric Research is sponsored by the National Science Foundation. Special thanks to I. Ermolli and T. Holzer.

References

Avrett, E.H. 1992, SOLER22 Workshop, p. 20
Caballero-Lopez, R.A., et al. 2004, JGR, 109, A12102
Dickinson, R.E. 1975, BAMS, 56, 1240
Fontenla, J., et al. 1999, ApJ, 518, 480
Fröhlich, C., & Lean, J. 2004, A&A Rev, 12, 273
Gleeson, L.J., & Axford, W.I. 1968, ApJ, 154, 1011
Jackman, C.H., et al. 1999, Adv. Space Res., 24, 625
Jackman, C.H., et al. 2001, GRL, 28, 2883
Jokipii, J.R. 1991, in *The Sun in Time*, p. 205
Kazil, J., & Lovejoy, E.R. 2004, JGR, 109, D19206
Kelley, M.C. 1989, *The Earth's Ionosphere*, San Diego: Academic Press
Lockwood, J.A., & Webber, W.R. 2005, JGR, 110, A04102
Lockwood, M. 2005, in *The Sun, Solar Analogs and the Climate*, p. 109
Low, B.C. 1996, Solar Phys., 167, 217
Marsch, N.D., & Svensmark, H. 2000*a*, Phys. Rev. Lett. 85, 5004
Marsch, N., & Svensmark, H. 2000*b*, SSRv 94, 215
McCracken, K.G., et al. 2001*a*, JGR, 106, 21585
McCracken, K.G., et al. 2001*b*, JGR, 106, 21599
Ogurtsov, M.G., et al. 2004, Solar Phys., 222, 177
Parker, E.N. 1958, ApJ, 128, 664
Parker, E.N. 1965, P&SS, 13, 9
Reames, D.V. 1999, SSRv, 90, 413
Reid, G.C., Solomon, S., & Garcia, R.R. 1991, GRL, 18, 1019
Rusch, D.W., et al. 1981, P&SS, 29, 767
Schrijver, C.J., & Zwaan, C. 2000, *Solar and Stellar Magnetic Activity*, Cambridge: Cambridge Univ Press
Shaviv, N.J. 2002, Phys. Rev. Lett., 89, 051102
Simunac, K.D.C., & Armstrong, T.P. 2004, JGR, 109, A10101
Spruit, H.C. 1976, Solar Phys., 50, 269
Sun, B., & Bradley, R.S. 2002, JGR, 107, 4211
Svensmark, H., & Friis-Christensen, E. 1997, J. Atmos. Sol. Terr. Phys., 59, 1225
Thuillier, G., Joukoff, A., &, Schmutz W. 2003, ISCS Symposium 23, ESA SP-535, 251
Tinsley, B.A. 2000, SSRv, 94, 231
Woods, T.N., et al. 2005, JGR, 110, A01312
Yashiro, S., et al. 2004, JGR, 109, A07105